Low Cloud Detection for the GOES ABI using a Random Forest Classifier

John M. Haynes[1], Yoo-Jeong Noh[1], Steven D. Miller[1], and Andrew K. Heidinger[2]

(1) Cooperative Institute for Research in the Atmosphere, Fort Collins, CO (2) NOAA/NESDIS, Madison, WI | Email: john.haynes@colostate.edu

Introduction

- Passive remote sensing instruments like the Advanced Baseline Imager (ABI) on GOES-16/17, are particularly effective at revealing attributes of the topmost layer of clouds (their height, particle size, water content, etc.). However in multilayer situations, information on those lower layers is limited.
- NOAA customers, however (particularly in the aviation community), may be particularly interested in the presence of low clouds. This is especially relevant for general aviation in terms of applicability of VFR vs. IFR conditions, the presence of aircraft icing, mountain obscuration, etc.

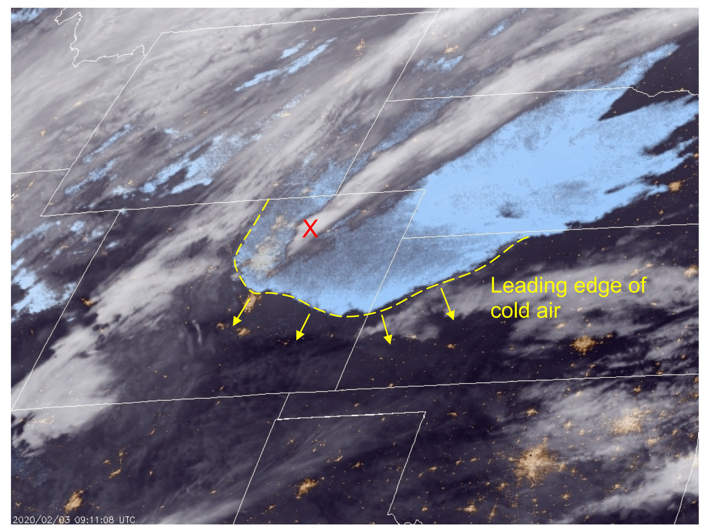

GOES-16: GeoColor image of cold air outbreak on 2020/02/03
(IR [white] + background city lights + low cloud [blue] 10.3-3.9 µm)

- The ABI satellite image at left shows a cold air outbreak spreading southward across the Great Plains. Low clouds are occurring behind the front in the cold air.
- The white/gray areas are high clouds identified by their cold IR brightness temperatures; the blue areas are low clouds detected using a 10.3 minus 3.9 µm threshold.
- Are there low clouds "hiding" under the cirrus at the red 'X'? *Our meteorological experience says "yes", but this isn't at all evident from a satellite algorithm alone.*

- The purpose of this study is to explore the use of Machine Learning to improve our ability to detect low clouds from satellites, especially to augment existing satellite products.

Original (non-ML) Cloud Product

- The baseline cloud height identification product that we wish to improve is called Cloud Cover Layers (CCL). In its earliest form, this algorithm identified ABI pixels as containing exactly one of (**L**)ow, (**M**)id, or (**H**)igh cloud, based mostly on the associated cloud top height determination.
- In the past three years, we have improved this product by using *a priori* statistical relationships derived from the spaceborne CloudSat radar and CALIPSO lidar (Noh et al. 2017) to derive the geometric thickness of the topmost cloud layer (**Δ**z) for any pixel observed by the ABI. When combined with the cloud top height (CTH), this new information allows cloud to occupy more than one vertical level. The following diagram demonstrates how a cloud that used to be simply classified as H (high) can now be classified as H+M (high plus mid):

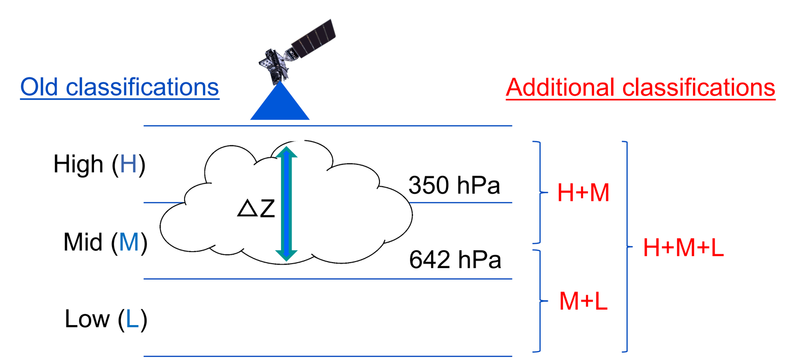

Figure shows old and new cloud classifications. Note that CCL allows six cloud categories:

H,M, L, H+M, M+L, and H+M+L.

It cannot accommodate *low clouds under high clouds* (H+L), because no cloud breaks are allowed

- We can evaluate this algorithm using overpasses of the CloudSat radar and CALIPSO lidar through the ABI full disk sector. This is an example vertical cross section through some clouds that ABI-only algorithms identified as containing *only cirrus*:

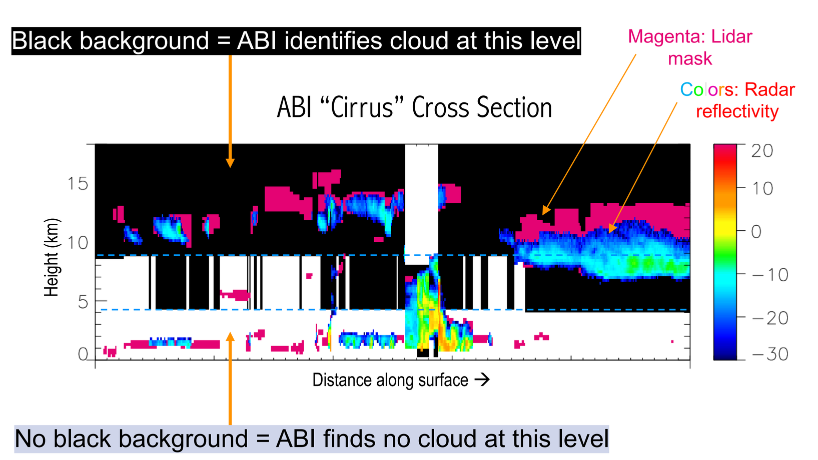

- The radar/lidar reveal that there is significant coverage of low clouds (below 4 km) in scenes that ABI indicates contains only cirrus.
- These low clouds are largely *not resolved* by the ABI CCL algorithm (as indicated by lack of a "black background" in low levels)
- **More rigorously, we find that although ABI CCL can identify about 73% of low clouds, this drops to 22% when such clouds occur under cirrus.**

Data / Preprocessing

- We want to improve the ABI Cloud Cover Layers product by "filling in" the missing low clouds (see bottom left panel of this poster) using machine learning.
- CloudSat radar and CALIPSO lidar will provide the "truth"; as active sensors, they detect most clouds in the atmosphere.

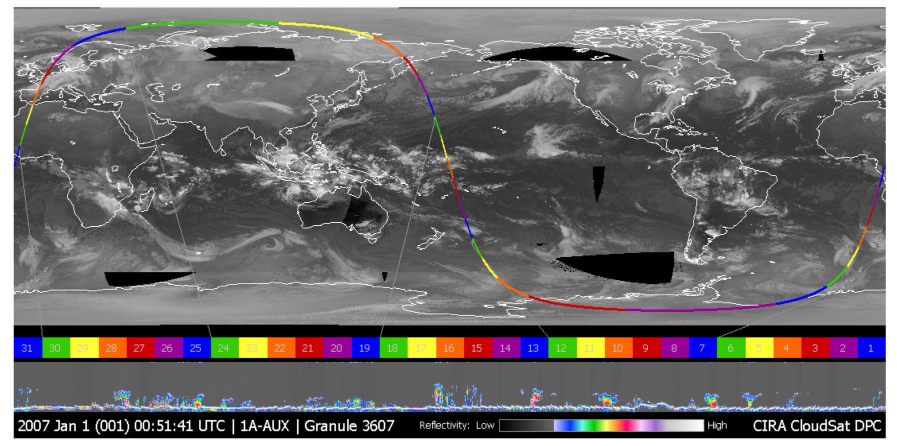

One orbit of CloudSat (colored lines) overlaid on a geostationary infrared "collage" background

CloudSat/CALIPSO radar and lidar data were matched to GOES ABI observations for 141 days in 2017 and 2019, for a total of 9.9 million radar profiles

7.8 million profiles are used for algorithm training, and the rest are reserved for testing

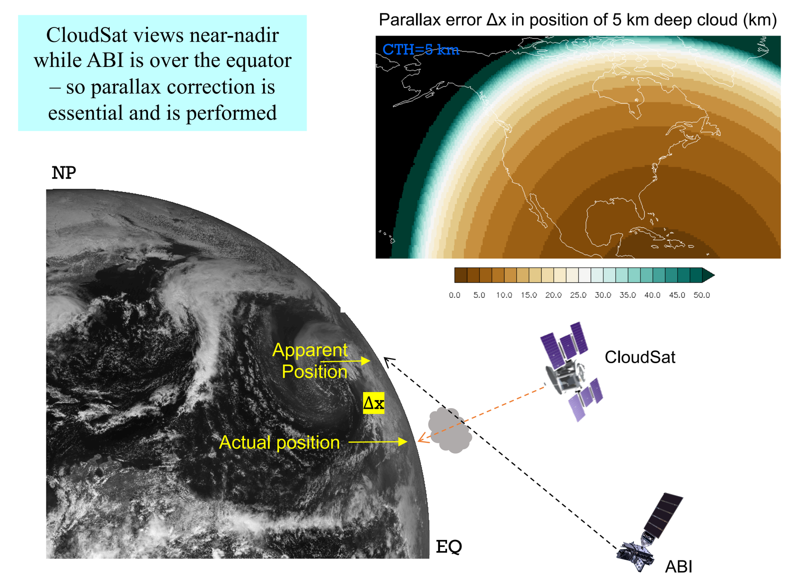

- The parallax-corrected GOES-16 ABI data are matched to the nearest pixel along CloudSat / CALIPSO ground track, in all 16 channels
- Currently, surrounding pixels are not utilized (but we expect improvements by doing so)
- National Snow and Ice Data Center (NSIDC) daily microwave SSM/I-based land/sea surface characterization, the GTOPO30 elevation map, and atmospheric relative humidity profiles from ECMWF model are also matched to the same location

Method

- A Random Forest (RF) classifier (Breiman 2001) is used for this work. For each of the matched CloudSat/CALIPSO/ABI pixels in the training set, the binary question is asked "Is a low cloud (< 642 hPa) present?"
- Data used for training has been determined experimentally. Initially we included all ABI channels in the training, but a selection of physically relevant channels, ratios, and differences has led to better results.
- Currently we use the following for training during daytime:

ABI channels 1-3,7,10,14 (0.47, 0.64, 0.87, 3.9, 7.34, 11.2 µm)	
TB 10.35 µm – TB 12.3 µm	TB 3.9 µm – TB 11.2 µm
1.38 / 0.64 µm reflectance ratio	Solar zenith angle
Surface elevation in meters	Latitude
ECMWF profiles of relative humidity in layers: 0-1.9 km, 1.8-4 km, 4-6.2 km	
Surface characterization flag (0=unknown, 10=open sea, 20=sea ice, 30=frozen land or sea)	

- At night, training data does not use channels ≦ 3.9 µm

Example motivations behind just a few of these choices…

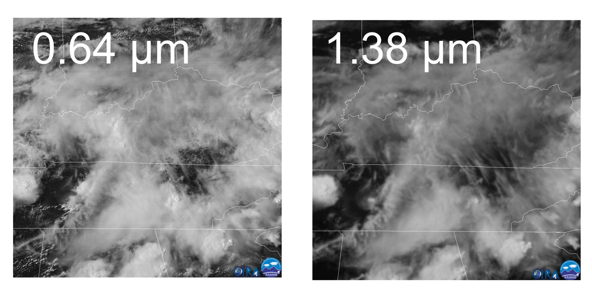

1.38 / 0.64 µm reflectance ratio

1.38 um is in a water vapor absorption band; low clouds tend to preferentially "disappear" at 1.38 compared to 0.64 um due to low level water absorption

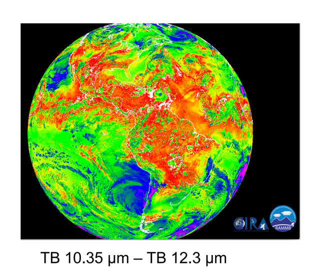

Split window difference

The 10.35 minus 12.3 µm split window difference has long been used as a cloud classifier, e.g. Purbantoro et al. (2018)

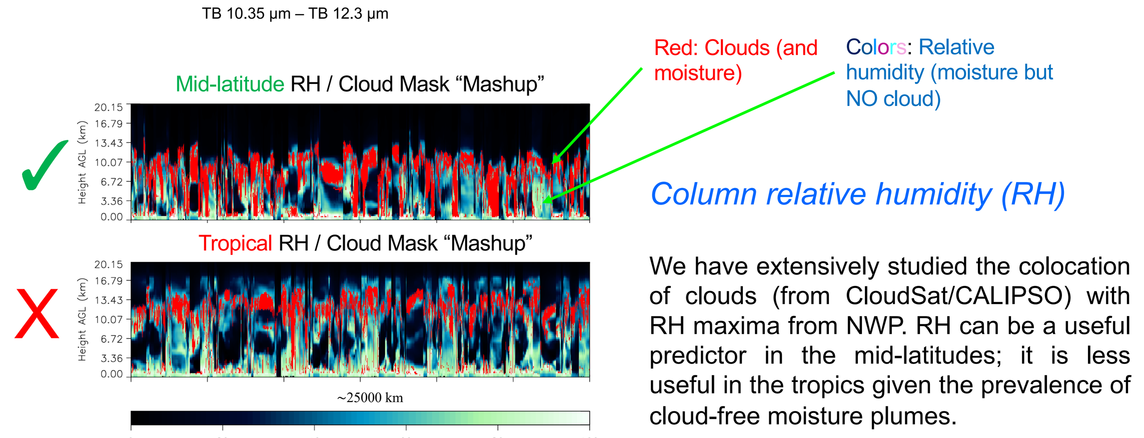

Column relative humidity (RH)

We have extensively studied the colocation of clouds (from CloudSat/CALIPSO) with RH maxima from NWP. RH can be a useful predictor in the mid-latitudes; it is less useful in the tropics given the prevalence of cloud-free moisture plumes.

Results

- After training, the daytime results are evaluated on an independent test data set, consisting of 2.1 million CloudSat/CALIPSO/ABI matchups (Oct 2017, Jan 2019)
  - **Inputs**: ABI / ECMWF / NISE / DEM data from table at left
  - **Outputs**: Is there cloud below 642 hPa? (0 or 1)
  - **Validation**: CloudSat / CALIPSO radar lidar "truth"
- In these runs, 50 estimators (trees) are used; but there is practically no improvement (or degradation) in evaluation on the test data set after ~25 estimators

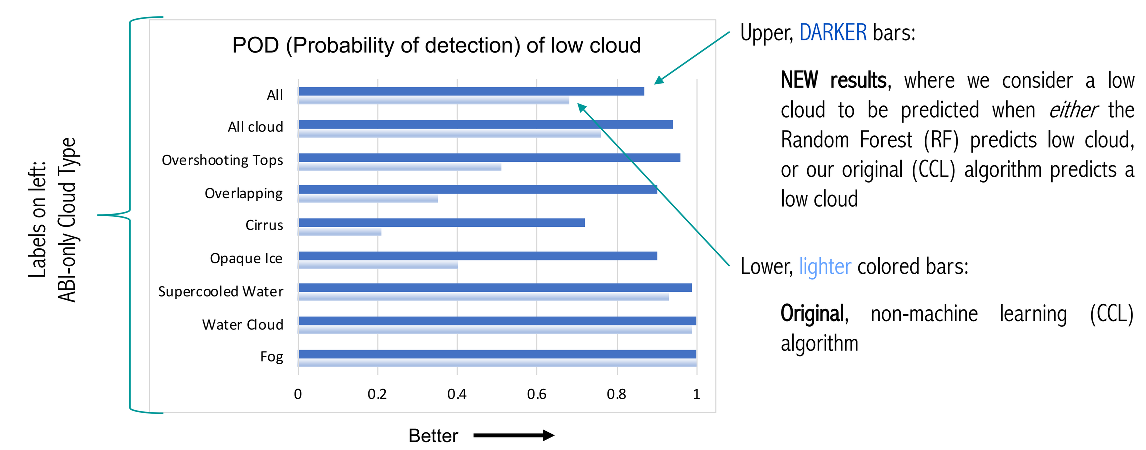

Figure at left shows that the new algorithm (dark bars) has increased POD compared to the original algorithm (light bars) for all cloud types (except same for fog)

Improvement is most significant for the Cirrus and Overlapping cloud categories, which contain a significant fraction of multilayer clouds.

The RF algorithm has learned radiance and humidity profiles associated with low cloud occurrence (RH is not part of the original algorithm).

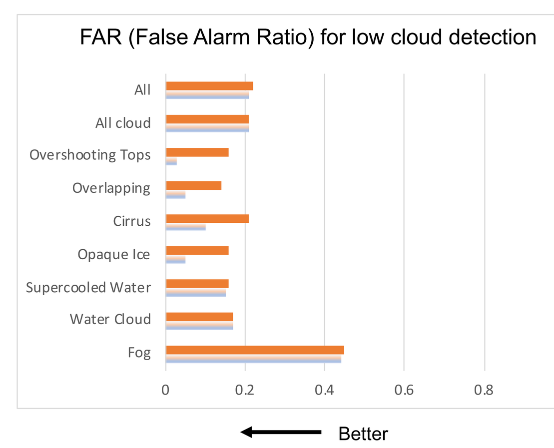

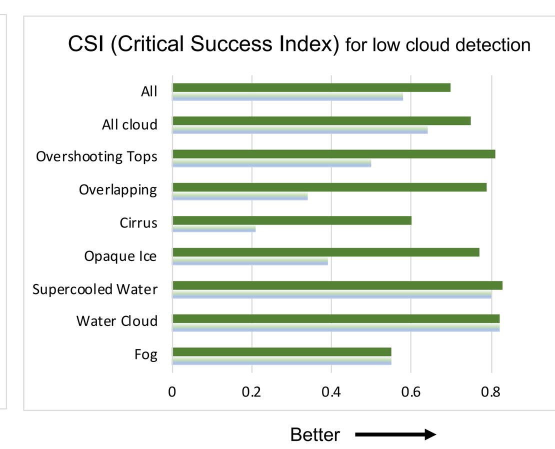

Figures at far-left show the FAR for low cloud detection for the new algorithm (dark bars) and original algorithm (light bars), for all ABI cloud types.

Note that the new algorithm has an increased rate of false alarms (detecting low cloud where there is none), for the same categories that simultaneously show the largest detection improvements. This is not particularly surprising, as the original algorithm is unable to identify the heights of broken cloud layers in multilayer scenes.

CSI (a non-linear combination of POD and FAR) increases for all categories.

Feature Importance

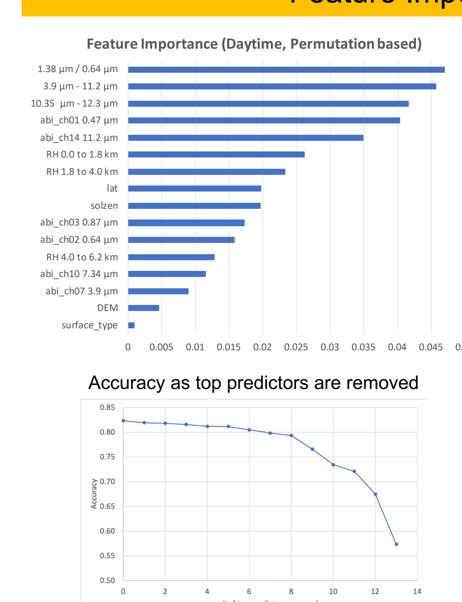

Permutation-based feature importance analysis shows that the 1.38/0.64 reflectance ratio, 3.9-11.2, and 10.35-12.3 channel differences have the largest influence on the trained model.

However ABI channels are highly correlated with one another, as demonstrated by the slow decrease in accuracy when top predictors are independently removed, one-by-one, and training repeated.

This suggests an operational retrieval can be run with a decreased # of inputs, while retaining similar accuracy.

Two Examples of the Improved Algorithm

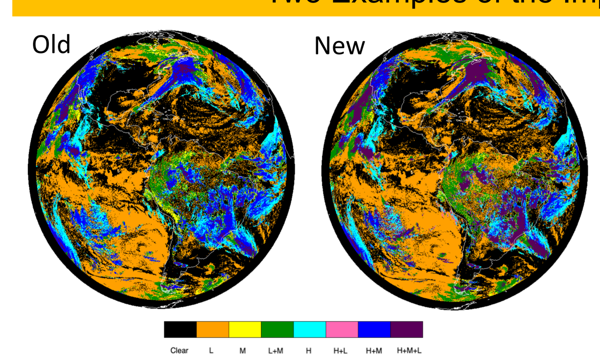

Figure shows a full-disk GOES-16 image of the original (left) and new RF-informed (right) CCL algorithm from 2019/01/05 17:15 UTC.

Note especially the shift from **H**igh+**M**id cloud to **H**igh+**M**id+**L**ow cloud (blues → purples) in the deepest cyclones. This is consistent with CloudSat radar sampling of such systems.

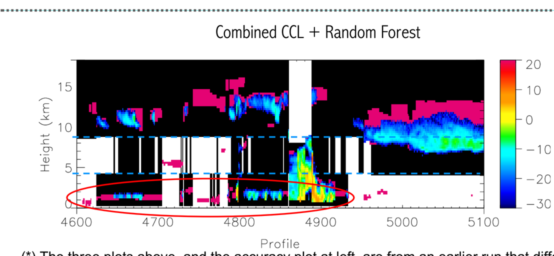

This is the same cross-section through ABI-identified cirrus as shown in the bottom-left figure of this poster; except the black background (showing levels where the CCL algorithm determines clouds are present) has been updated with the low cloud RF output.

Note that the low level clouds are now largely properly detected, whereas they were missed before.

(*) The three plots above, and the accuracy plot at left, are from an earlier run that differs only in that it does not include surface elevation or surface characterization

Data:
GOES ABI courtesy NOAA
CloudSat, CALIPSO, and ECMWF data from CIRA's CloudSat Data Processing Center: http://www.cloudsat.cira.colostate.edu
Microwave-based surface data characterization from National Snow and Ice Data Center: https://nsidc.org
Digital elevation (GTOPO30) data from United States Geological Survey: https://www.usgs.gov

References:

Breiman, L., 2001: Random forests. *Mach. Learn.*, **45**, 5–32, https://doi.org/10.1023/A:1010933404324.
Noh, Y.-J., and Coauthors, 2017: Cloud-base height estimation from VIIRS. Part II: A statistical algorithm based on A-Train satellite data. *J. Atmospheric Ocean. Technol.*, **34**, 585–598, https://doi.org/10.1175/JTECH-D-16-0110.1.
Purbantoro, B. and Coauthors, 2018: Comparison of cloud type classification with split window algorithm based on different infrared band combinations of Himawari-8 satellite. ARS, 07, 218–234, https://doi.org/10.4236/ars.2018.73015.